

Delivering interlaminar reinforcement in composites through electrospun nanofibres

T. R. Pozegic, S. G. King, M. Fotouhi, V. Stolojan, S. R. P. Silva & I. Hamerton

To cite this article: T. R. Pozegic, S. G. King, M. Fotouhi, V. Stolojan, S. R. P. Silva & I. Hamerton (2019) Delivering interlaminar reinforcement in composites through electrospun nanofibres, *Advanced Manufacturing: Polymer & Composites Science*, 5:4, 155-171, DOI: [10.1080/20550340.2019.1665226](https://doi.org/10.1080/20550340.2019.1665226)

To link to this article: <https://doi.org/10.1080/20550340.2019.1665226>



© 2019 The Author(s). Published by Informa UK Limited, trading as Taylor & Francis Group.



Published online: 19 Sep 2019.



Submit your article to this journal [↗](#)



Article views: 428








View related articles [↗](#)



View Crossmark data [↗](#)

Delivering interlaminar reinforcement in composites through electrospun nanofibres

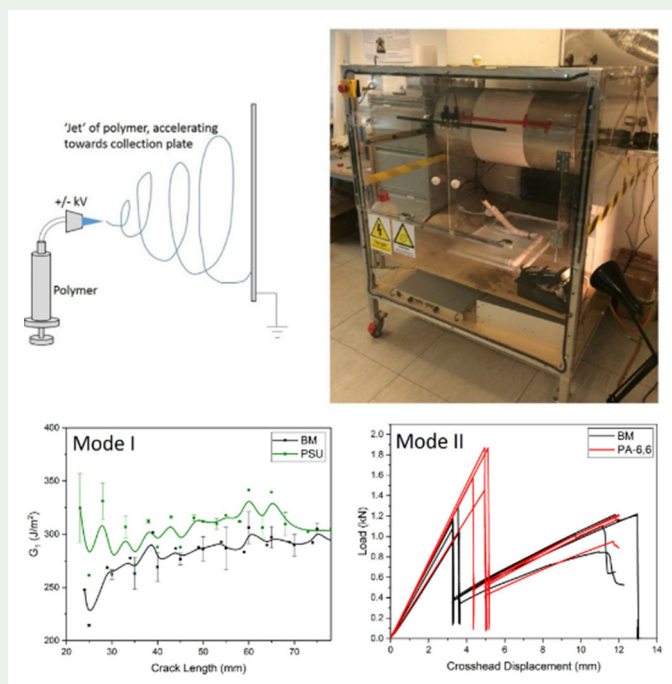
T. R. Pozegic^a , S. G. King^b , M. Fotouhi^a , V. Stolojan^b , S. R. P. Silva^b  and I. Hamerton^a 

^aDepartment of Aerospace Engineering, School of Civil, Aerospace, and Mechanical Engineering, Bristol Composites Institute (ACCIS), University of Bristol, Queen's Building, University Walk, Bristol, UK; ^bAdvanced Technology Institute, Department of Electrical and Electronic Engineering, University of Surrey, Guildford, Surrey, UK

ABSTRACT

Electrospun nonwoven veils comprising thermoplastic fibres (average diameter 400–600 nm) based on polysulfone (PSU), polyamide (PA-6,6), and polyetherimide (PEI) have been fabricated and used as interlaminar reinforcements in carbon fibre composites containing a commercial epoxy resin (8552/IM7). Samples were tested for their interlaminar properties and improvements were observed in the initial mode I interlaminar toughness of 30% (PA-6,6), 36% (PEI), and 44% (PSU), while improvements of 7% (PSU) and 8% (PEI) were observed in the propagation of the mode I interlaminar toughness. A reduction of 11% was observed for the propagation of the mode I interlaminar toughness for PA-6,6. Post-testing analysis of the cross-section and the fracture surface revealed that the crack front avoids the reinforcement significantly for PA-6,6. For mode II, however, this failure mechanism leads to improvements of 30% in interlaminar toughness for the PA-6,6, whereas the other reinforcements display negligible (PEI) and 31% reduction (PSU) interlaminar toughness.

GRAPHICAL ABSTRACT



ARTICLE HISTORY

Received 16 April 2019
Accepted 30 August 2019


KEYWORDS

Interlaminar; electrospinning; nanofibres; mode I; mode II; PA-6,6; PSU; PEI

1. Introduction

The list of successful applications in which composite materials have been employed has been increasing significantly year-on-year. Their attractive low-

weight, high tensile properties, combined with a high corrosion resistance, has led to adoption in items from as small as protective mobile phone cases, to those as large as jumbo-sized aircraft.

CONTACT T. R. Pozegic  t.pozegic@bristol.ac.uk  Bristol Composites Institute (ACCIS), Department of Aerospace Engineering, School of Civil, Aerospace, and Mechanical Engineering, University of Bristol, Queen's Building, University Walk, Bristol BS8 1TR, UK

*Present address: School of Engineering, University of Glasgow, Glasgow, G12 8QQ, Scotland

© 2019 The Author(s). Published by Informa UK Limited, trading as Taylor & Francis Group.

This is an Open Access article distributed under the terms of the Creative Commons Attribution License (<http://creativecommons.org/licenses/by/4.0/>), which permits unrestricted use, distribution, and reproduction in any medium, provided the original work is properly cited.

Table 1. Selection of modes I and II results from literature, highlighting improvements and reductions in interlaminar properties.

Interleaf	Ref.	$G_{Ic,i}$	$G_{Ic,p}$	$G_{IIc,i}$
PA-6,6	[9]	152%	31%	109%
	[24]		–41%	
	[25]		–22%	
	[26]			
SBS	[27]	90%		
PCL	[28]	94%	27%	
	[12]			7%
PAI	[12]	–58%	–68%	
	[29]			56%
PVA	[13]	–12%		
PVDF	[29]			57%
PES	[12]			20%
PVB	[12]			–6%

Recent reports predict the global end-product market of composites is expected to reach \$113.2 billion by 2022 [1]. Of these, perhaps the most widely recognized amongst the general public are carbon fibre reinforced polymers (CFRP). Despite a list of impressive properties, these materials are generally poor in the resistance to delamination initiation and propagation, thus poor in impact resistance. Unfortunately, these failure modes are difficult to monitor [2]. One particular mode of failure, composite delamination, may lead to loss of stiffness, compressive residual strength, development of local stress concentrations, and instability, further developing the delamination. Therefore, enhancements in these areas are of critical importance to composite research and applications.

Numerous strategies have been employed to try and alleviate composite delamination weakness such as: laminate stitching [3], use of fuzzy fibres [4], critical ply termination [5], matrix toughening [6], and edge cap reinforcement [7]. However, most of these methods have detrimental effects on other physical/manufacturing properties, such as: increased laminate thickness, poor resin flow, non-uniform reinforcement distributions, and reduction of the in-plane mechanical properties [4, 8–10]. A promising solution, with fewer compromises, is the incorporation of a polymer interlaminar reinforcement, more specifically (although not exclusively), a nonwoven nanofibre veil [11]. Compared to conventional microfibrils, nanofibres provide a number of advantages, for instance: high porosity, which is critical for the necessary impregnation and wet-out of the fibre reinforcement [12], and a high surface-to-volume ratio enhancing interfacial adhesion. Given the relative brittleness of the thermoset matrix, upon interlaminar crack formation, it has been demonstrated that the presence of a ductile thermoplastic non-woven interlayer provides an effective resistance to crack initiation and propagation [13].

Electrospinning is a common method for the production of non-woven nanofibres [13]. It

employs high voltages to electrostatically accelerate viscoelastic polymer solutions from a spinneret to a target, uniaxially stretching the fibres until solidification. Nanofibre production *via* electrospinning is a well-established industrial technique and, being a relatively versatile process, it is currently utilised for a large range of applications, including: structural materials (including textiles [14]), composites [15], energy [16], filtration [17], and biological (cell and tissue growth and drug delivery) [18, 19]. As a method to improve the interlaminar properties of a composite, electrospinning offers many benefits over other techniques for producing nanofibres, providing engineering controls over parameters such as: fibre orientation [20], fibre diameter [21], crystallinity [22], porosity, inclusion of nano-structures [23], and surface-to-volume ratio; it is suitable for solvents with low volatility (for instance, polar aprotic solvents such as dimethyl sulfoxide (DMSO), b.p. 189 °C at 1 atm.).

A selection of polymers has been implemented as nanofibre veil reinforcements. Polyamide 6,6 (PA-6,6) [12, 13] has been a popular option and is commercially offered by Revolution Fibres Ltd. (e.g. Xantu.Layr[®]). The popularity of polyamide is founded on the fact that it is relatively inexpensive, easily processable, has superior mechanical properties to other potential polymer candidates and has a melting point (268.8 °C) greater than the curing point of most thermoset matrices [13]. A recently published review by Palazetti *et al.* [13] has compiled mechanical testing results on polymeric nanofibre modifications. To review, a selection of results, where the methodology is similar to that presented in this work will follow. For clarity, see Table 1.

The addition of PA-6,6 as a non-woven interlaminar toughening interleaf has resulted in improvements in the mode I performance; for instance Shivakumar *et al.* [9] reported enhancements of 152 and 31% in $G_{Ic,i}$ and $G_{Ic,p}$, respectively, where $G_{Ic,i}$ is the critical mode I interlaminar toughness at the initiation point and $G_{Ic,p}$ is the critical mode I interlaminar toughness during propagation. However, reductions in interlaminar toughness were also reported for PA-6,6; both Daelemans *et al.* [24] and Alessi *et al.* [25] saw reductions in $G_{Ic,p}$ of 41 and 22%, respectively. Other polymers have displayed enhancements: poly(styrene-*co*-butadiene-*co*-styrene) (SBS) displayed 90% improvements in $G_{Ic,i}$ for glass fibres [27] and polycaprolactone (PCL) displayed 94% and 27% improvements in $G_{Ic,i}$ and $G_{Ic,p}$ (for glass fibres), respectively [28]. In the latter case, interestingly, van der Heijden *et al.* observed greater improvements with a double fibre interleaf than a single interleaf. Reductions were also observed by polymers: poly(amide-imide) (PAI) displayed 58% and

68% reductions in $G_{Ic,i}$ and $G_{Ic,p}$, respectively [12] and poly(vinyl alcohol) (PVA) displayed a 27% reduction in $G_{Ic,i}$ [13]. Crack propagation between both sides of the interlaminar reinforcement have been observed leading to nanofibre bridging [30] and thus increasing the energy required for delamination. For mode II, improvements in $G_{IIc,i}$ of: 109% have been reported for PA-6,6 [26]; poly(vinylidene difluoride) (PVDF)—57% [29]; PAI—56% [12]; polyethersulfone (PES)—20% [12]; and PCL—7% [12]. However, poly(vinyl butyral) (PVB) was reported to display a reduction in mode II performance of 6% [12]. Liu *et al.* [31, 32] determined the optimum thickness of epoxy 609 nano-reinforcement to be 70 μm (for mode I) and 128.1 μm (for mode II).

Evidently, there are discrepancies and mixed results when employing interleaves in the interlaminar region. This could be a consequence of the variability of interleaf fabrication or how the interleaf co-exists with the composite. Furthermore, although the results listed are closely related to the work in this article, there are variables that are inconsistent (number of plies, testing methodology, for example).

In this publication, we explore the effects of a range of interlaminar reinforcement veils using high-performance polymers; polysulfone (PSU) and polyetherimide (PEI), chosen, because of their compatibility with epoxy resin and a commercially available interlaminar reinforcement product, Xantu.Layr[®]. The Xantu.Layr[®] veils used had an areal weight of 1.5 g/m², which at this loading, has been reported to increase mode I fracture toughness by 173% and mode II interlaminar fracture toughness by 69% [33].

Both PEI and PSU polymers were electrospun to produce a nonwoven nanofibre veil, before being incorporated into a unidirectional prepreg CFRP composite. All composites, along with benchmark samples (based on HexTow IM7 fibres and HexPly 8552 epoxy) containing no reinforcement veil were then subjected to quasi-static modes I and II failure testing. The cross-sections of the delaminated samples were further investigated, using scanning electron microscopy.

PEI (ULTEM[®] 1000), is an amorphous thermoplastic (specific gravity: 1.27) with a T_g of 217 °C. It is defined by the aromatic imides which are incorporated with ether linkages which provide chain flexibility [34]. PA-6,6 (specific gravity: 1.14) is a semi-crystalline, aliphatic polymer with repeating amide linkages with a T_g of 50 °C. PSU (Udel[®]) is an amorphous thermoplastic (specific gravity: 1.24) with a T_g of 190 °C. It is composed of 1,4-phenylene units linked by isopropylidene, ether, and sulfone moieties. The high degree of resonance, as a consequence of the sulphone group and the benzene ring, results in the polymer having high strength.

However, flexibility in the backbone provided by the ether linkage moderately augmented by the isopropylidene linkages imparts toughness.

2. Methodology

2.1. Materials

All materials used in this study were used as received, without further purification or modification. *N*-Methyl-2-pyrrolidinone (NMP) and *N,N'*-dimethylformamide (DMF), were purchased from Sigma Aldrich (Merck). Polysulfone (Udel[®] Bisphenol A PSU) was supplied by Solvay (Wilton, UK) and polyetherimide (ULTEM[®] 1000, PEI) was acquired from Plastics International. The electrospun polyamide (PA-6,6, Xantu.Layr[®], 1.5 g/m²) interlaminar veils were supplied by Revolution Fibres Ltd. [35]. The carbon fibre prepreg was composed of HexPly 8552 (toughened epoxy) and HexTow IM7 (intermediate modulus carbon fibre) obtained from Hexcel.

To prepare each of the electrospinning solutions, the chosen polymers were dissolved over 12 hours under constant magnetic stirring at room temperature. To produce the PEI nanofibres, 20 wt.% PEI was dissolved in NMP [36]; to produce the PSU nanofibres, 20 wt.% PSU was dissolved in a 1:1 mixture of DMF and NMP [37, 38]. The nanofibres were electrospun with a set-up consisting of a Glassman power supply connected to an in-house built single needle electrospinning rig, positioned perpendicular to a high-speed cylindrical rotating collector, with the polymer solutions pumped using a Chemyx OEM syringe pump. To produce the PSU nanofibres, the needle was subjected to a potential difference of +15 kV, with the solution pumped at 700 μl per hour; whereas to produce the PEI nanofibres, the needle was subjected to a potential difference of +18 kV, with the solution pumped at 600 μl per hour, in order to avoid needle 'blobbing'. In each case, the spinneret was positioned approximately 15 cm from a rotating collector (300 rpm). The atmospheric conditions during both electrospinning sessions were controlled by an air handling unit at a temperature of 21 °C, and a relative humidity between 31 and 34%.

Four (300 × 300 mm²) laminates were fabricated—150 × 140 mm² for double cantilever beam (DCB) testing (Figure 1), 150 × 160 mm² for end-notched flexure (ENF) testing. Of these, half were reinforced with the nanofibre interleaf; the other half served as benchmarks (BM). The lay-up was [0]₂₄ using Hexcel IM7/8552 and cured following the manufacturer's instructions. All samples were cut using a diamond saw and prepared in accordance with ASTM guidelines.

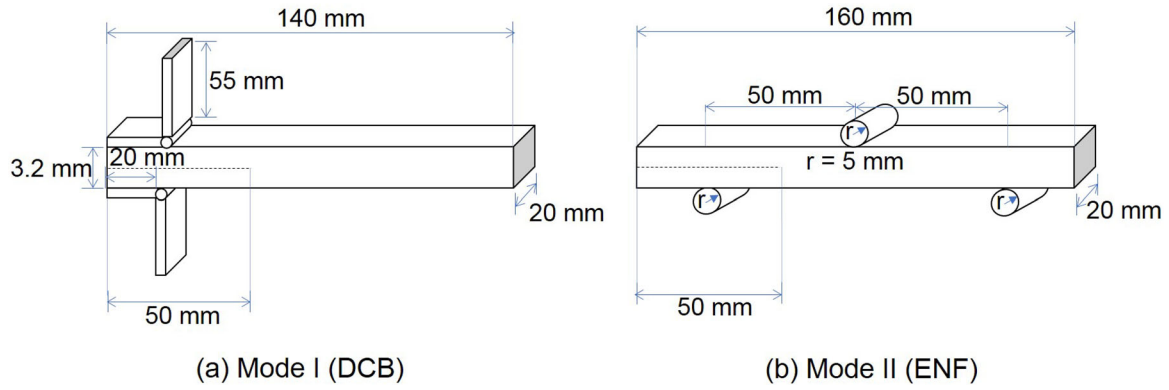


Figure 1. Nominal dimensions are stated for (a) mode I, double cantilever beam and (b) mode II, end-notched flexure configurations. Dashed lines within samples represent the nonadhesive insert, 'r' represents radius.

The DCB procedure described in this work followed the ASTM (2007) guidelines [39], of nominal size of $(140 \times 20) \text{ mm}^2$ composed of $[0]_{24}$, IM7/8552 plies. A schematic diagram of the DCB sample used for the test is shown in Figure 1. The initial crack was created by laying a 20 μm polyimide (PI) nonadhesive film 50 mm from the end of the samples in the centre plane. Steel hinges were adhered to the sample using an epoxy adhesive (DP490, 3M). A Shimadzu AGS-X (1 kN load cell) testing instrument was used with a cross-head displacement rate of 1 mm/min. Crack propagation was monitored using a standard DSLR camera in video mode and data were collected at a rate of 10 Hz. Samples were not pre-cracked as the initial fragmentation (without pre-cracking) has been reported to provide additional information on the veil's performance [33].

The Modified Beam Theory (MBT) was chosen for the data reduction method, as recommended by the ASTM D 5528 standard [39]. In this method, the strain energy release rate (G_{Ic}), is corrected for the rotation at the delamination point as follows:

$$G_{Ic} = \frac{3P\delta}{2b(a + |\Delta|)} \quad (1)$$

where P is the load; δ is the load point displacement; b is the sample width, and a is the crack length from the load point. By creating a least squares plot of the cube root of compliance as a function of the delamination length, Δ can be determined by the value of the x -axis intercept. Given the samples did not display large deflections, high interlaminar fracture toughness or low flexural modulus, no additional corrections were made.

ENF samples were fabricated with the same fibre/matrix as the DCB specimens—IM7/8552, with $[0]_{24}$ plies and with a polyimide interleaf placed 50 mm from the end of the specimen. The length was marked with white corrective paste and allowed to dry completely to enable the paint to fracture in a

brittle manner. An Instron 8872 mechanical testing instrument was used, with a 10 kN load cell and operated at 1 mm/min.

The mode II fracture toughness can be evaluated as [40, 41]:

$$G_{IIc,i} = \frac{9a^2P_c\delta_c}{2B(2L^3 + 3a^3)} \quad (2)$$

where δ_c is the critical deflection at the loading point; L is the specimen half-span; a is the delamination length, P_c is the critical load, and B is the specimen width.

To observe how the crack propagated along the mode I and II test samples, a representative sample of each reinforcement and the benchmark were cut along the width by a diamond saw at two locations: one directly at the crossover point of the nonadhesive film and the sample or veil reinforcement (G_{Ic}) and a second, 25 mm beyond the first ($\sim G_{Ip}$). The samples were polished using a Buehler EcoMet 250 Pro, with the following polishing procedure: Buehler P400 SiC for 4 min (water cooled), P1200 SiC for 4 min (water cooled), 1 μm diamond suspension on polishing pad for 4 min, and 0.3 μm diamond suspension on polishing pad for 4 min. For all, the load applied was 25 N and the platen and head speed were 150 and 40 rpm, respectively. The samples were cleaned using distilled water. The cross-sections of the samples were analyzed in a Hitachi TM3030 at 15 kV with a combined backscattered and secondary electron detector. To observe the fracture surfaces, the entire tested length of representative mode I and II samples were divided in three sections, sputter coated with Ag to prevent charging, and analyzed using a SEM (JEOL IT300) at 15.0 kV with a secondary electron detector. SEM images of the nanofibers were taken using a FEI Quanta 200 operating at 20 kV.

3. Results

The electrospun PSU and PEI nanofibres were analysed before incorporation into the composites,

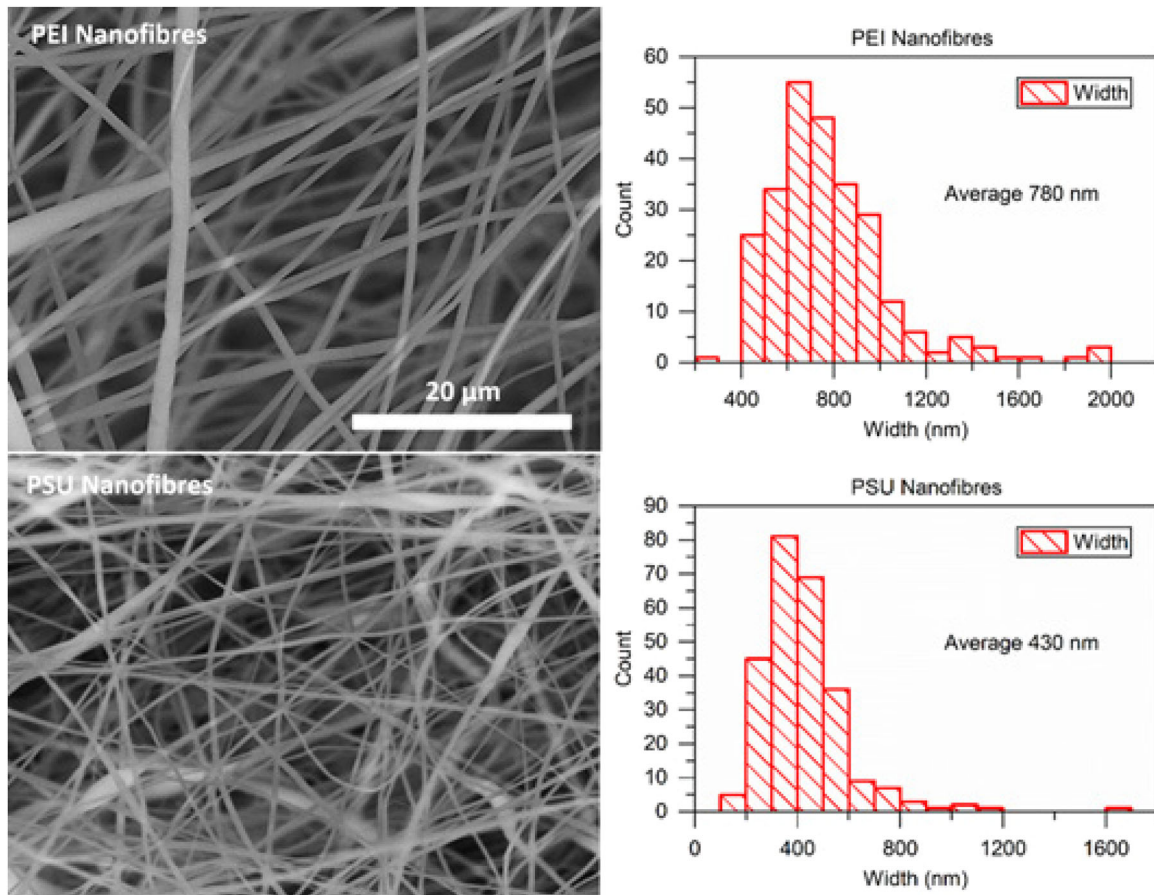


Figure 2. SEM micrographs of the electrospun PEI and PSU nanofibres, combined with their corresponding histograms of the measured nanofibre diameters. The average diameter of the PEI nanofibres was 780 ± 20 nm, whereas for the PSU nanofibres it was 430 ± 10 nm.

allowing any differences to be highlighted. It has been observed that there are no advantages to electrospinning straight on to the carbon fibre as opposed to collecting the fibres and laying up during the lay-up procedure [13]. The SEM micrographs of the resulting PEI and PSU nanofibres (Figure 2) revealed that the average diameters were 780 ± 20 and 430 ± 10 nm, respectively. The measured nanofibre areal weights for each veil were 11.8 and 12.2 g/m^2 , for PEI and PSU, respectively, which is over an order of magnitude greater than the commercially available Xantu.Layr[®] (1.5 g/m^2). Although a matched areal weight for each veil would have been ideal, in this case this was not possible, due to the limited supply of material available at the time of testing. Around 12 g/m^2 was chosen for our electrospun veils (PSU and PEI) as it was an average for all of the previous veils tested where areal weight was reported [9, 12, 24, 27, 28].

In total, three of each: benchmark (no reinforcement), PSU, PEI, and PA-6,6 reinforcements were tested for the interlaminar fracture toughness (G_I) by progressing a mode I fracture in a DCB configuration.

Crack propagation with a sharp crack front was progressive with fibre bridging in all samples, albeit of varying amounts (Figure 3). Fibre bridging is a

well-reported phenomenon that enhances interlaminar toughness and is typically only seen in unidirectional fibre specimens [4]. A small correlation between fibre bridging and the interlaminar fracture toughness was observed in this work.

Figure 4 displays the raw data of load against the crosshead displacement. The maximum loads achieved for the BM are more consistent than the interlaminar reinforced specimens. For each of the interlaminar reinforced sample types, there is an increase in the maximum load in comparison to the benchmark. In addition, there is a different response post-maximum load for the interlaminar reinforced samples, this has been emphasised with Figure 4(ai–ci). Evidently, all interlaminar reinforced samples have suppressed the delamination, by minimizing the load drop, post-initial fragmentation.

Figure 5 displays the G_I results for uncorrected (a–c) and following correction for rotation at the delamination point (ai–ci) for the BM, PA-6,6, PEI, and PSU, respectively; after the initial crack, the G_I is steady. As expected, the corrections have reduced the interlaminar toughness of the specimens, but interestingly, have subdued the enhancements in PEI and PSU that were observed, pre-correction. To improve the analysis of the results, the G_I was

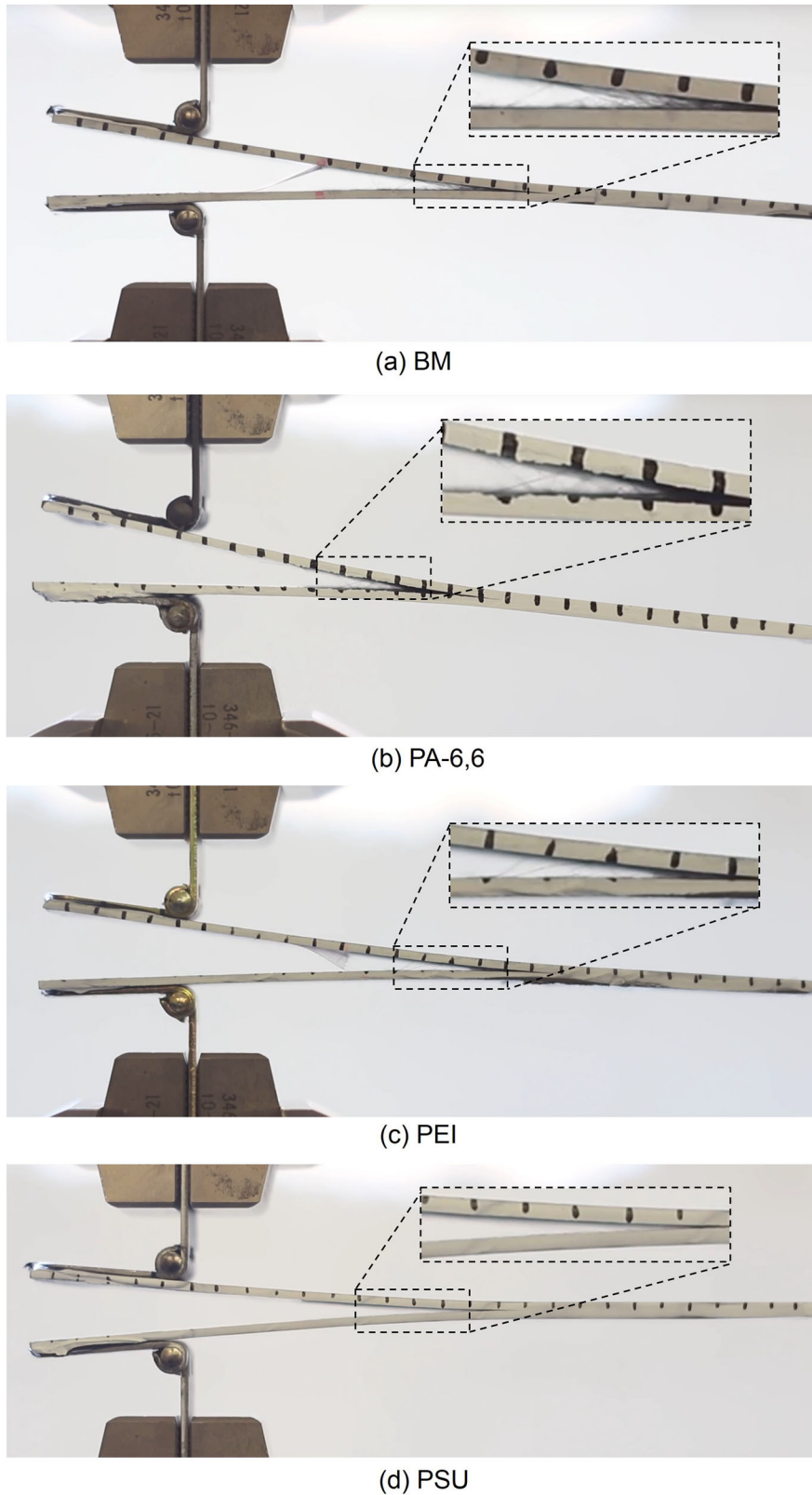


Figure 3. DSLR photographs of the fractured mode I specimens undergoing testing, highlighting the fibre bridging (see inserts).

averaged for each sample and compared. The average results are shown in Figure 6, along with a table of results comparing $G_{Ic,i}$ and $G_{Ic,p}$ (Table 2). For PA-6,6, there exist only two points prior to 30 mm (Figure 5(ai)), hence the absence of error bars in Figure 6(a). The averaged $G_{Ic,i}$ in Table 2 is

averaged from the first initial points of each and is therefore reflective of the $G_{Ic,i}$ of the material. The G_{Ic} of the benchmark specimens reported in this work are in line with those reported by Czabaj *et al.* [42], who similarly used the IM7/8552 pre-preg configuration and the same data reduction method.

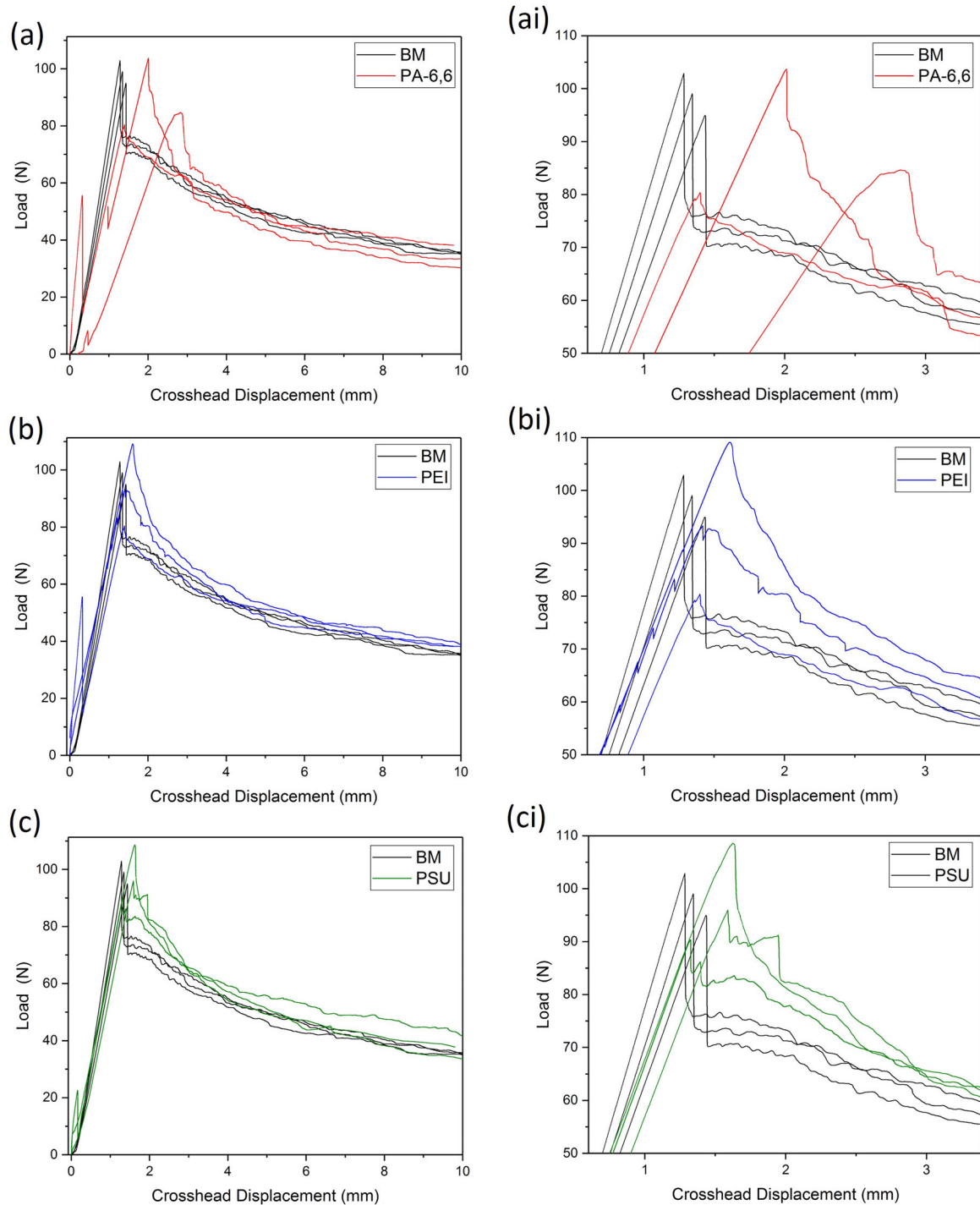


Figure 4. Load against crosshead displacement for all specimens. BM is characterised by a greater reduction in load after the maximum loads, whereas the interlaminar reinforced samples are characterized by a more gradual reduction in load post-maximum load. Initial load drops at ~ 55 N in (a) and (b); ~ 20 N in (c) are attributed to the hinge adhesive migrating to the mid-plane crack. (For interpretation of the references to colour in this figure legend, the reader is referred to the web version of this article).

Considering the initial fracture toughness, all interlaminar reinforced samples displayed an improvement. PA-6,6 displayed a $G_{IC,i}$ of 293 ± 43 J/m², a 30% increase over the benchmark sample (225 ± 11 J/m²), whereas PSU displayed a 44% improvement (to 325 ± 32 J/m²) and PEI displayed a 36% improvement (to 307 ± 42 J/m²). During the crack propagation, this enhancement reduces and in the case of the PA-6,6 reduces by 11% (to 257 ± 12 J/m²). PSU and PEI maintain a small enhancement of 7 and 8%,

respectively. This reduction in fracture toughness propagation was also observed elsewhere in PCL [28], PA-6,6 [9, 12, 25, 43], PVB [12], and PAI [12]. Beckermann *et al.* [33] also observed that after the initial fracture, $G_{IC,p}$ are very similar between all samples, subsequently, they concluded that $G_{IC,i}$ is more indicative of the enhancements gained through a reinforcing veil. Considering the PA-6,6, the improvements in $G_{IC,i}$ of 30% compare well with literature where improvements range from 23 to 152% [9, 12, 24, 43].

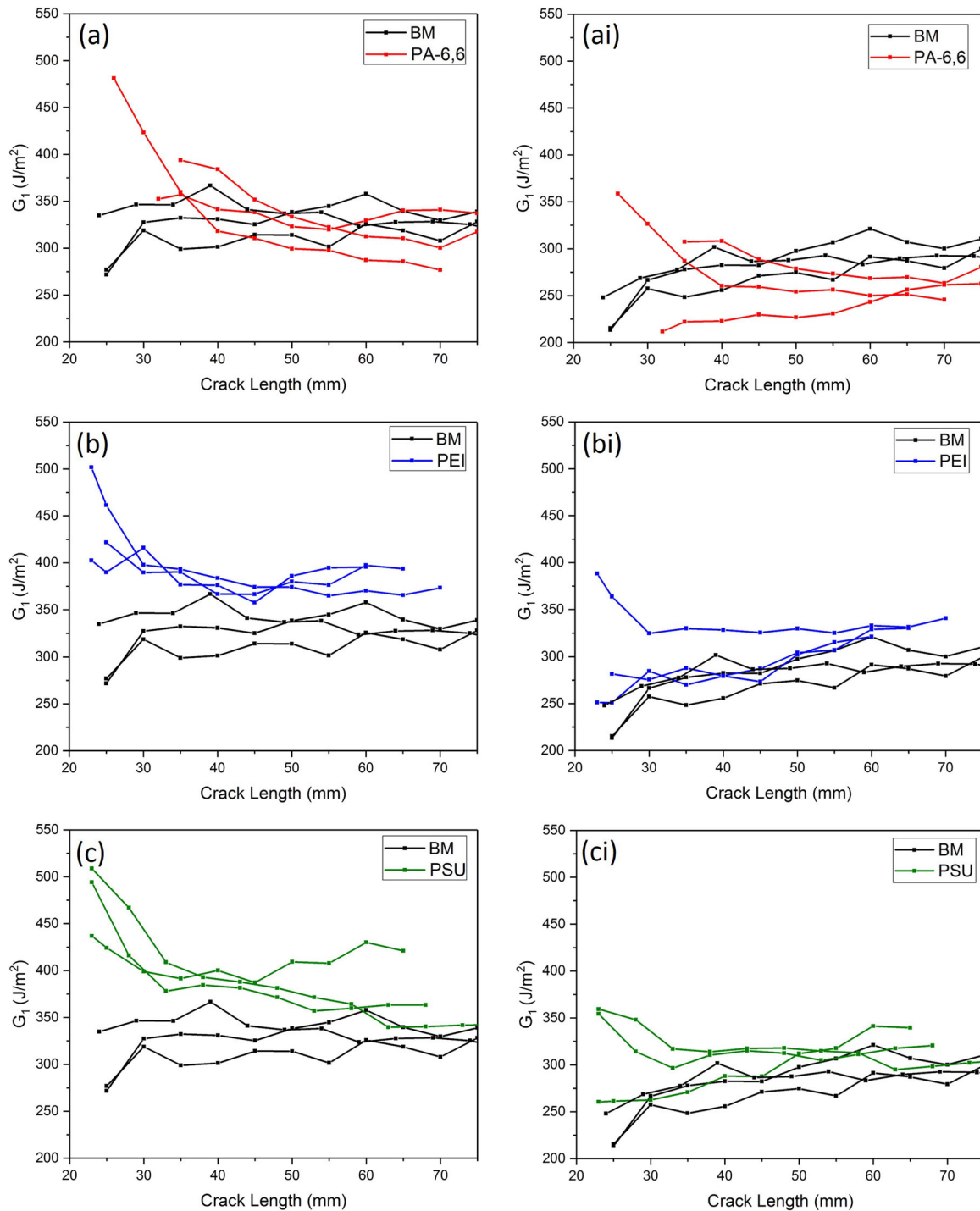


Figure 5. Comparison of mode I samples, (a–c) uncorrected (ai–ci) rotation corrected with comparisons against BM samples for (a–ai) PA-6,6, (b–bi) PEI, and (c–ci) PSU DCB samples. (For interpretation of the references to colour in this figure legend, the reader is referred to the web version of this article).

The reduction observed in $G_{I,c,p}$ are also reported elsewhere, where reductions range from -41% to -6% [12, 24], although improvements of 11% [43] and 31% [9] have been observed.

Kim *et al.* [44] previously published tests performed on PEI interleaves in mode I using the MBT and reported a $G_{I,c,I}$ value of 1.5 kJ/m^2 , however, this was conducted for a homogeneous thermoplastic matrix composite using a bidirectional 5 harness satin weave reinforcement, which, for the latter case, is expected to result in higher toughness values [43].

Li *et al.* [45] observed a 180% increase in interlaminar performance when they electrospun a nanofibrous PSU membrane directly on the carbon fibre epoxy pre-preg. Li *et al.* observed greater enhancements from the nanofibrous addition as opposed to a $30 \text{ }\mu\text{m}$ film and was attributed to the heterogeneous phase separation of the nanofibres during curing of the epoxy resin.

As previously mentioned, the response of the load to crosshead displacement of benchmark is in contrast to the interlaminar reinforced samples

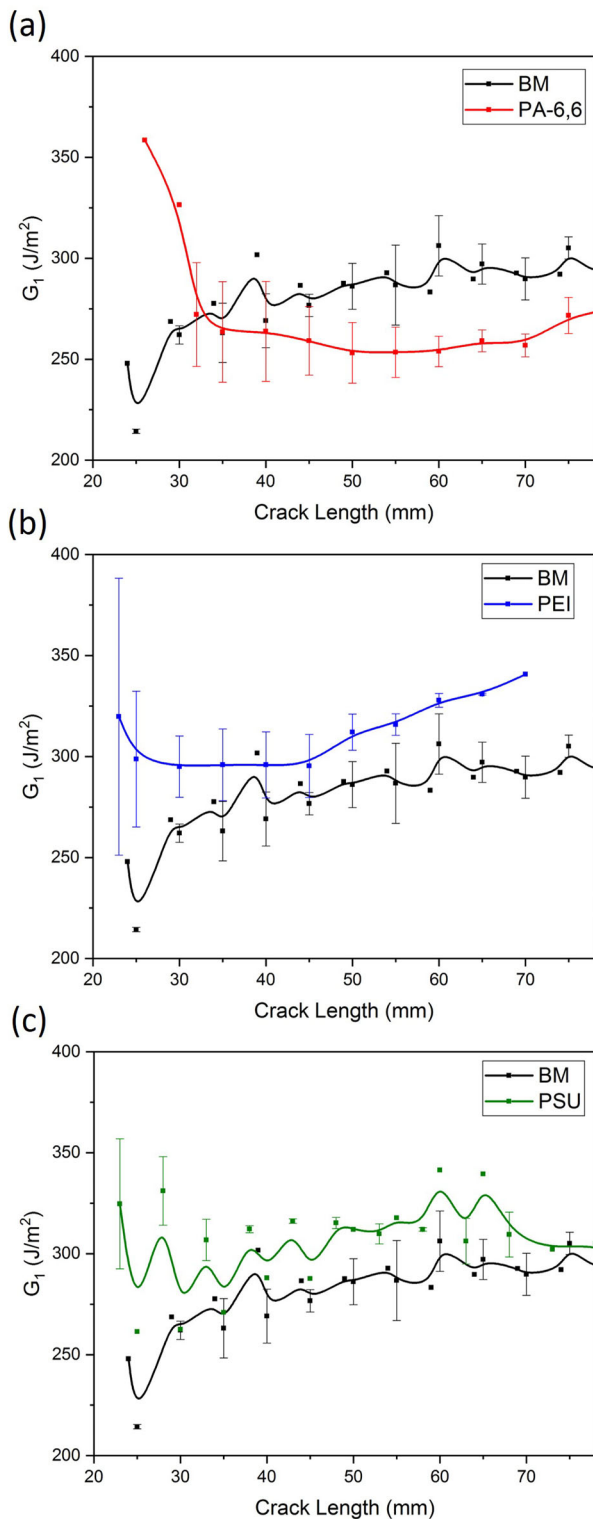


Figure 6. Combined results, rotation corrected, with comparisons against BM samples for (a) PA-6,6, (b) PEI, and (c) PSU, with a b-spline fit. (For interpretation of the references to colour in this figure legend, the reader is referred to the web version of this article).

beyond the initial fragmentation. By comparing the G_{IC} results to the load data, the consequence of the progressive load drop characteristics of the interlaminar reinforced samples on the G_{IC} can be assessed. For clarity, a representative sample of each type is compared in Figure 7, with the initial fracture emphasised. Whereas the G_{IC} of BM shows an

Table 2. Mode I values of interlaminar modified composites.

Material	$G_{IC,i}$ (J/m ²) (% delta)	$G_{IC,p}$ (J/m ²) (% delta)
Benchmark	225 ± 11	288 ± 8
PA-6,6	293 ± 43 (+30%)	257 ± 12 (−11%)
PEI	307 ± 42 (+36%)	312 ± 1 (+8%)
PSU	325 ± 32 (+44%)	308 ± 12 (+7%)

increase beyond the initial fracture, the interlaminar reinforced samples show a decrease. Apart from PA-6,6 (Figure 7(b)), all interleaf reinforced samples plateau to a greater G_{IC} value compared to BM.

Evidently, there is still scope for improvements in interlaminar enhancements from nanofibre interleaves. Brugo *et al.* [43] observed that, during crack propagation in the unidirectional specimen, the crack deviated away from the toughening interleaf; for the complex plain weave carbon fibre composite, the complex morphology of the fabric hindered the progression of the crack along the fibre–matrix interface, diverting it into the toughened interleaf. Similarly, the undulating morphology of the plain weave configuration leads to an undulating interleaf (as also observed in the cross-section analysis), requiring additional energy to delaminate. Their conclusion was that the nano-reinforcement increases the initial fracture toughness, but the magnitude of $G_{IC,p}$ is dependent on the nature of the remaining composite fabric. Subsequently, SEM images of the width-by-thickness of the samples in this work were analysed to determine the crack propagation for each reinforcement compared to BM, and how the crack propagates along the length of the specimen.

Figure 8 displays the SEM cross-section of the crack in the vicinity of $G_{IC,i}$ (Figure 8(a–d)) and $G_{IC,p}$ (Figure 8(ai–di)) for each reinforcement and BM. There were fewer undulations in the crack front across the sample in the vicinity of $G_{IC,i}$; increasing as the crack propagated across the sample ($G_{IC,p}$), furthermore, there was more evidence of multiple crack fronts propagating along the length of all samples, including intra-ply fracture (i.e. Figure 8(ai, bi, and ci)). The most striking observation was for PA-6,6 (Figure 8(b and bi)); the crack front had avoided the interlaminar reinforcement (see dashed red line) at the initial fracture point and had propagated in adjacent inter/intra-ply zones. Such features have been reported elsewhere [43]. This was not seen for the other interlaminar reinforcements, PEI and PSU (Figure 8c–ci and 8d–di, respectively).

The deviation of the crack front for PA-6,6 may explain the reduction in the $G_{IC,p}$ (Figure 6(a)), but this reduction leads to a $G_{IC,p}$ that is lower than the benchmark (257 ± 12 J/m² compared to 288 ± 8 J/m²). This result reinforces the findings in Figure 7, where there is evidence of potential deviation of the crack beyond the interleaf reinforced interlaminar region;

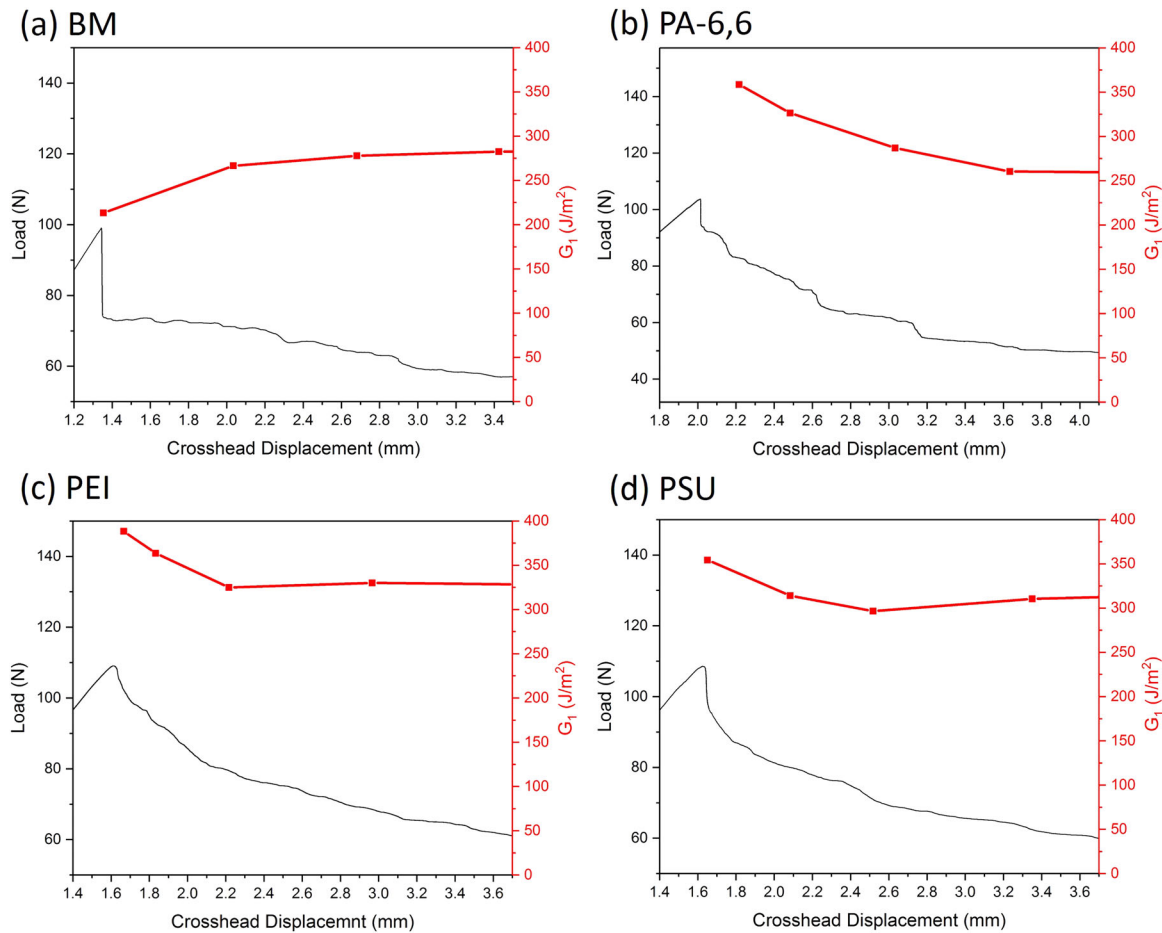


Figure 7. Load against crosshead displacement for representative samples of (a) BM, (b) PA-6,6, (c) PEI, and (d) PSU with the G_I . The figure emphasises the G_I post-initial load drop. It can be observed that the interlaminar reinforced samples are characterized with a gradual reduction in load in comparison to the benchmark. Note that the x-axis has been shifted to display the same region of the delamination for each specimens. (For interpretation of the references to colour in this figure legend, the reader is referred to the web version of this article).

the G_{Ic} is observed to converge with the BM beyond the initial crack. As mentioned, a characteristic of the nanofibre-reinforced samples is the progressive load drop suggesting that the crack is propagating along the reinforcement until it begins to deviate.

Photographs and SEM images of the fractured surfaces give further insight in the propagation of the crack during mode I delamination. In comparison to the BM (Figure 9(a)), PA-6,6 (Figure 9(b)) displays an inhomogeneous fracture surface alluding to the crack propagation transitioning from failure within the reinforcement to failure outside the reinforcement. PEI (Figure 9(c)), on the other hand, has a much smoother progression between these failure areas, whereas PSU (Figure 9(d)) is the only reinforcement which displays observable homogeneity at the fracture surface, suggesting the progressing crack front is efficiently engaged with the reinforcement. Both Figures 8 and 9 explain the reduction in improvement for the PA-6,6 reinforcement from $G_{Ic,I}$ to $G_{Ic,P}$ in comparison to BM; the propagating crack deviates away from the reinforcement. Figure 10 displays SEM images of the fracture surfaces and further reinforces the findings; the reinforced samples contain

a significant quantity of polymer on the fracture surface (Figure 10(b–d)). It is clear in Figure 10(b) for PA-6,6, how the crack has propagated through adjacent sections of the composite, leaving fibres exposed in the middle section of the image (inside of red dashed lines, Figure 10(b)). However, and although not shown, the polymer structures were fewer as the crack propagated along the sample.

The benchmark samples, and those containing PSU, PEI, and PA-6,6, were prepared in mode II ENF configuration. The raw data, representing the load against crosshead displacement for each sample type compared to BM samples, are shown in Figure 11. As can be seen in the figure, there is a linear increase in cross-head displacement until crack initiates beyond the non-adhesive insert, leading to a load drop. The load subsequently progresses linearly with cross-head displacement as the crack propagates along the sample. PA-6,6 (Figure 11) displays an observable improvement over the benchmark samples at the initial load drop, whereas PEI and PSU are observed to be comparable to the benchmark samples. The average maximum load observed of the benchmark is 1.15 ± 0.04 kN, PA-6,6 displays

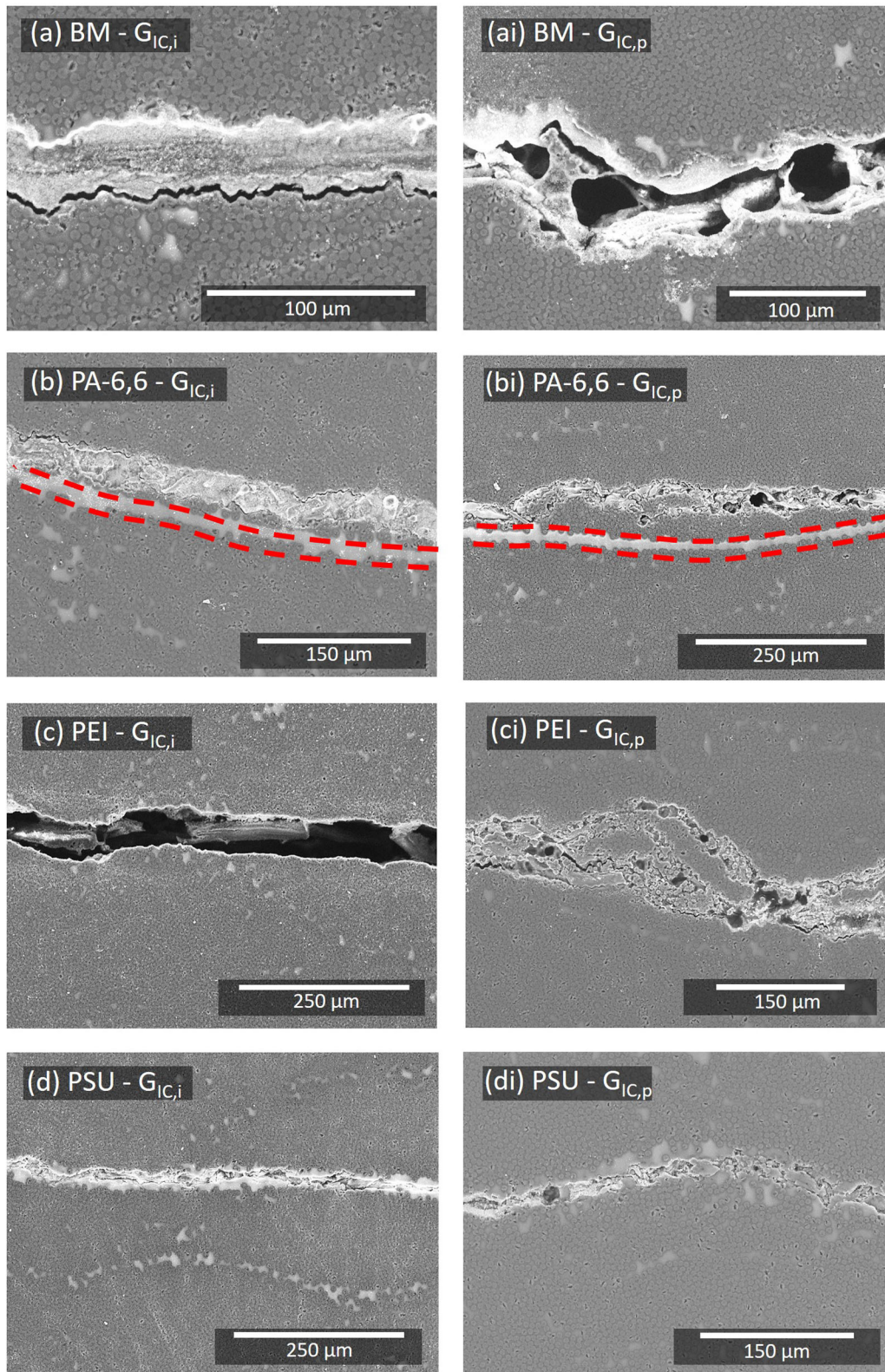


Figure 8. SEM images of the cross-section for DCB test samples at $G_{IC,i}$ (left, a–d) and $G_{IC,p}$ (right, ai–di). Red dashed line highlights the area of PA-6,6 reinforcement. (For interpretation of the references to colour in this figure legend, the reader is referred to the web version of this article).

a 47% enhancement (to 1.69 ± 0.10 kN) with PEI displaying a 23% enhancement (1.42 ± 0.06 kN). On average, PSU displays a reduction in maximum load of 8% (to 1.06 ± 0.08 kN). Using Equation 2, the $G_{IIC,i}$ reveals an average enhancement for PA-6,6 (369 ± 21 J/m²) of 30%, whilst PEI (281 ± 10 J/m²) displays no significant change (0.58%). PSU

displayed an average reduction in $G_{IIC,i}$ of 31% (to 196 ± 17 J/m²), compared to the benchmark (283 ± 12 J/m²). These results are compiled in Table 3. The similarity of the linear region beyond the first load drop of the benchmark and the interlaminar reinforced samples are consistent with the reinforcement offering no toughness enhancements,

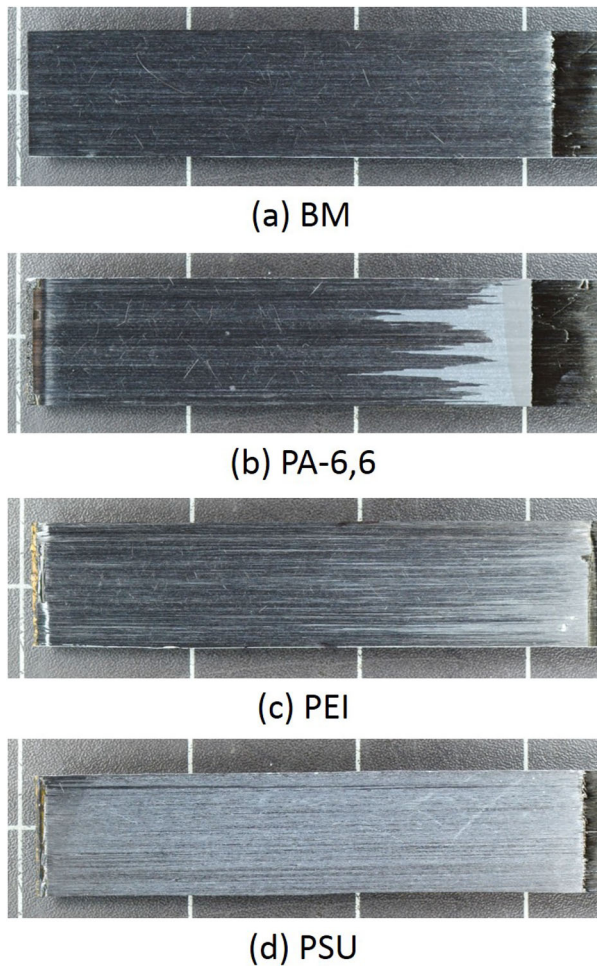


Figure 9. Photographs of the fracture surfaces of representative samples for each reinforcement type.

although interestingly, this region for the interlaminar reinforced samples is more consistently repeatable, compared to the benchmark and should be the focus of future work.

Using a similar expression to derive the $G_{IIc,i}$, Saghafi *et al.* [26] obtained a 109% improvement in $G_{IIc,I}$ for their PA-6,6 reinforced glass fibre-epoxy matrix composites. Furthermore, Palazetti *et al.* [13] states in their review that 15 out of 19 cases demonstrated improvements with nanofibre interleaf; one did not and four displayed unclear effects, suggesting that the results are inconsistent.

In comparison to the mode I results, the mode II results are in partial contrast. The $G_{IIc,i}$ results display the same trend as the $G_{IIc,i}$, however a reduction for PSU in mode II was observed (compared to the benchmark) and the magnitude of improvement of PEI for mode II is significantly less ($G_{IIc,i}$: 36%, $G_{IIc,i}$: 0.58% for PEI).

SEM images of the cross-section for ENF test samples at the initial ($G_{IIc,i}$) and propagated points ($G_{IIc,p}$) are displayed in Figure 12. Under mode II loading, the materials respond in a similar way as mode I, concluding that the crack front tends to avoid the reinforcement for PA-6,6 (Figure 12(b and bi)), unlike for PEI and PSU reinforcements. For PSU, a resin rich area can be observed (red dashed line, Figure 12(di)), with the crack passing through. There were no observable differences between the crack in the vicinity of $G_{IIc,i}$ and $G_{IIc,p}$.

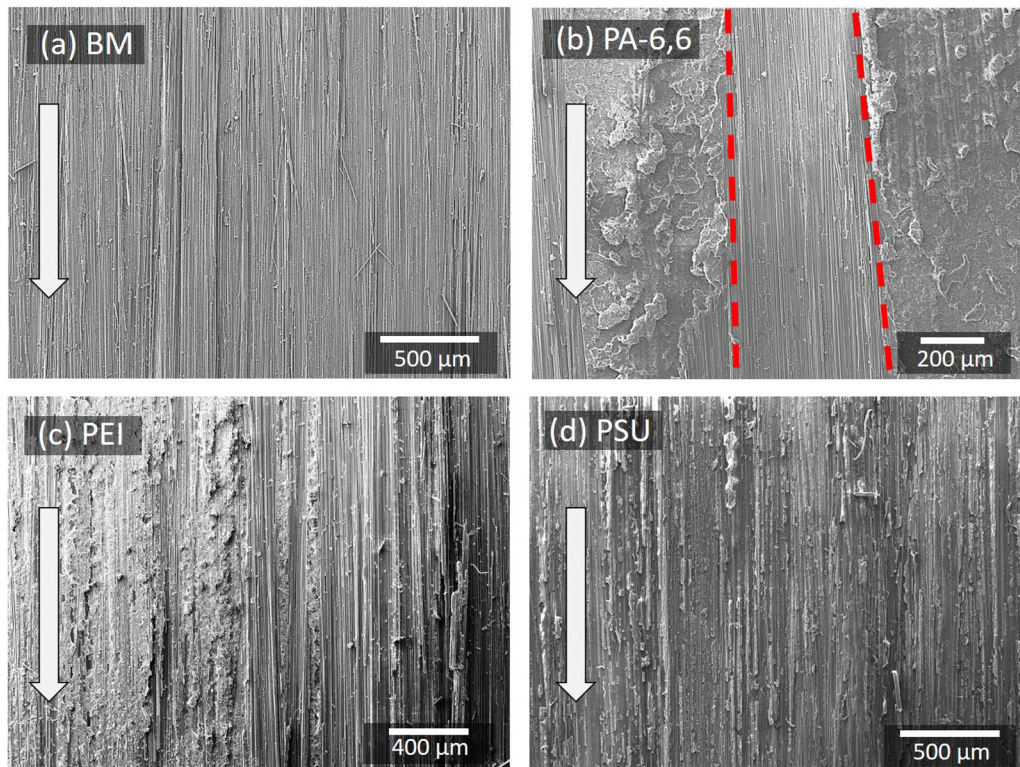


Figure 10. SEM images of the DCB fracture surfaces for (a) BM, (b) PA-6,6, (c) PEI, and (d) PSU. Red dashed lines highlight area of different failure mechanisms. The white arrow signifies the direction of crack propagation. (For interpretation of the references to colour in this figure legend, the reader is referred to the web version of this article).

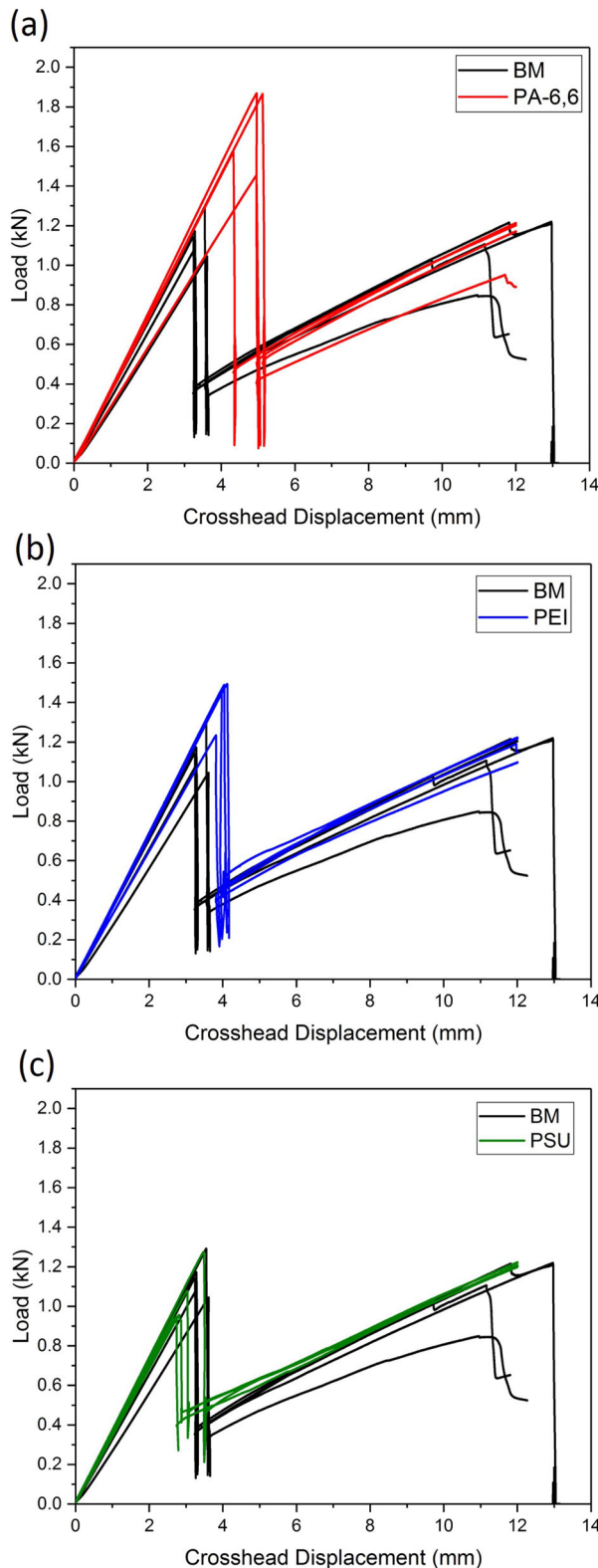


Figure 11. Load against crosshead displacement for each interlaminar reinforced composite compared to the BM. (For interpretation of the references to colour in this figure legend, the reader is referred to the web version of this article).

SEM images of the fracture surfaces of the ENF test samples are displayed in Figure 13. Shear hackles (green dashed box, Figure 13(ai)) were more abundant (or easily observable) for BM (Figure 13(a)), but can also be seen in PA-6,6, Figure 13(b). Shear hackles are attributed to tensile microcracks

Table 3. Mode II values of interlaminar modified composites.

Material	Average Max. Load (kN) (% delta)	$G_{IIc,i}$ (J/m ²) (% delta)
Benchmark	1.15 ± 0.04	283 ± 12
PA-6,6	1.69 ± 0.10 (47%)	369 ± 21 (31%)
PEI	1.42 ± 0.06 (23%)	281 ± 10 (0.58%)
PSU	1.06 ± 0.08 (−8%)	196 ± 17 (−31%)

in the epoxy resin matrix adjacent to the carbon fibres. As observed for the mode I tests, the crack front through PA-6,6 deviates through different sections, leaving observable clean fibres (outside of red dashed lines of Figure 13(bi)) and polymer structures in the centre (inside of red dashed lines Figure 13(bi)). Similarly, significant quantities of polymer can be seen in PEI (Figure 13(c)) and PSU (Figure 13(d)). As can be seen in Figure 13, the rupturing of carbon fibres has occurred (yellow dashed box in Figure 13(ai)) as an example, further resisting crack growth.

Whereas there are clear improvements in the initial fracture for both modes I and II (in particular for PA-6,6), there was evidence that the interlaminar reinforced samples resisted delamination—the improvement is reduced when the crack is propagating. As seen in Figures 8–10, 12, and 13, the crack front avoids the interleaf region which needs to be addressed. Beyond the initial load drop for the mode II tested samples, there seems to be insignificant differences between interlaminar reinforced and benchmark samples; the crack front avoiding the reinforcement—as with the mode I samples—could also be occurring. Further work will consider the compatibility and interaction of the interleaf and epoxy matrix during processing (i.e. curing). For example, Li *et al.* [45] noted the high viscosity of the PSF nanofibres and subsequently, poor diffusion of the PSF in the epoxy resin. Therefore, they dissolved the PSF leading to the formation of aligned spheres, leading to a 181% improvement in $G_{IC,p}$.

Future work should focus on understanding how the interleaf co-exists with the composite and whether the crack can be encouraged to propagate within the reinforcing region, this could be achieved by exploiting adjacent undulating plies, which have been shown to inhibit crack propagation away from reinforcement.

Unlike the other reinforcements, there was significant deviation of the crack front from the PA-6,6 interleaf. It should be noted that the PEI (11.8 g/m²) and PSU (12.2 g/m²) had a greater areal than the PA-6,6 (1.5 g/m²). This result suggests that even with a lower areal weight, the toughness of the PA-6,6 leads to the crack propagating into adjacent structures. This alternative failure mode hinders the performance of PA-6,6 reinforcing fibre composites for mode I crack propagation, but is advantageous under mode II loading.

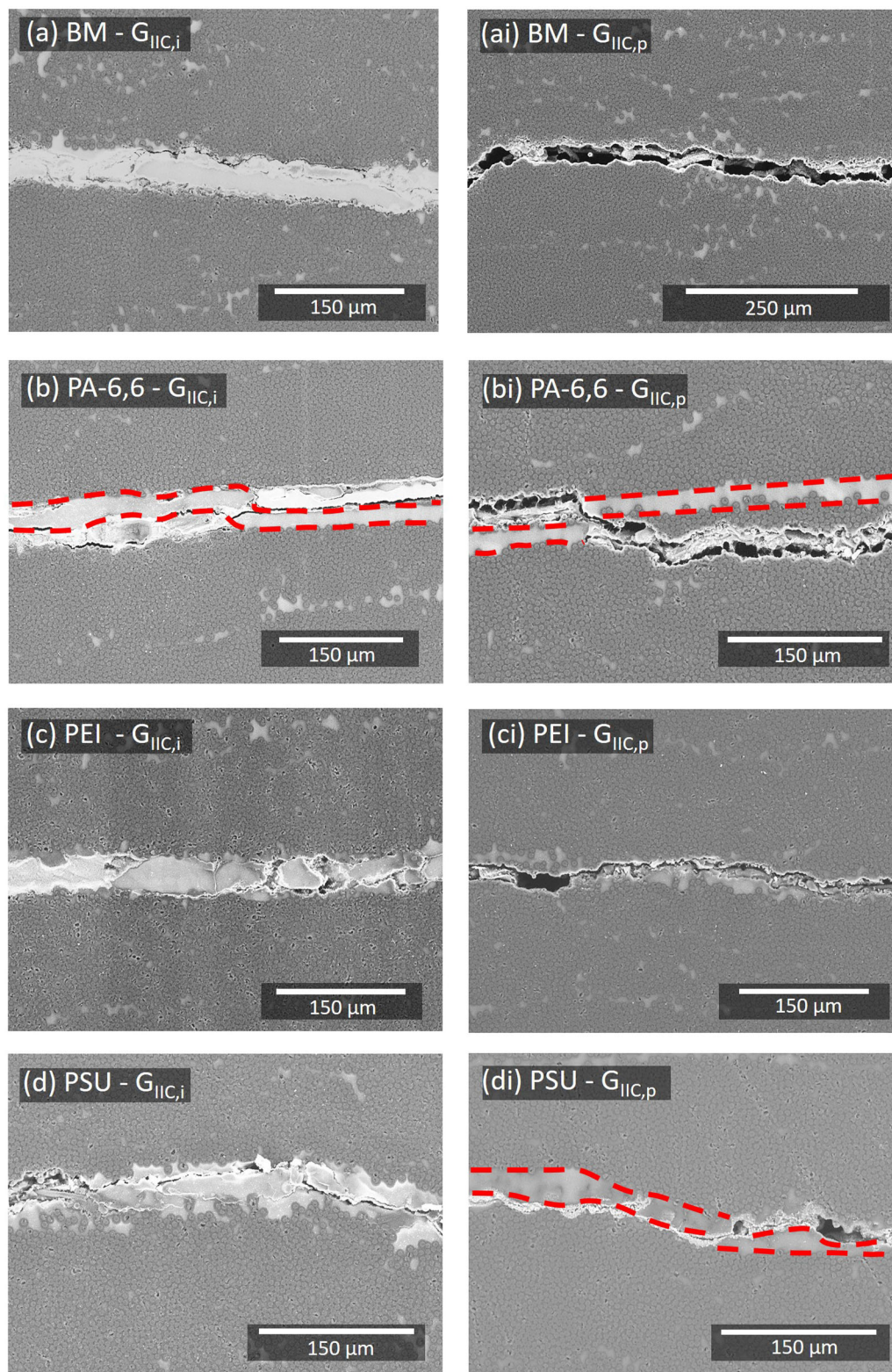


Figure 12. SEM images of the cross-section for ENF samples at $G_{IIc,i}$ (left, a–d) and $G_{IIc,p}$ (right, ai–di). Red dashed lines highlight interleaf reinforcement. (For interpretation of the references to colour in this figure legend, the reader is referred to the web version of this article).

Beckermann *et al.* [12] compared PA-6,6 veils with areal weights of 1.5, 4.5, and 9 g/m² and reported a linear increase (65%) of G_I from 1.5 to 4.5 g/m², but a significantly less increase from 4.5 to 9 g/m² (6.5%). There was a more complex behavior for G_{II} with areal weight; an increase (31%) from 1.5 to 4.5 g/m² with a reduction (8.7%) from 4.5 to

9 g/m². The results presented in this work demonstrate that PA-6,6 provides significant enhancements given the low areal weights. Further work should consider a greater range of areal weights of the PEI and PSU to examine the influence of areal weight to interlaminar toughening in comparison to PA-6,6 and whether PA-6,6 could be designed to encourage failure

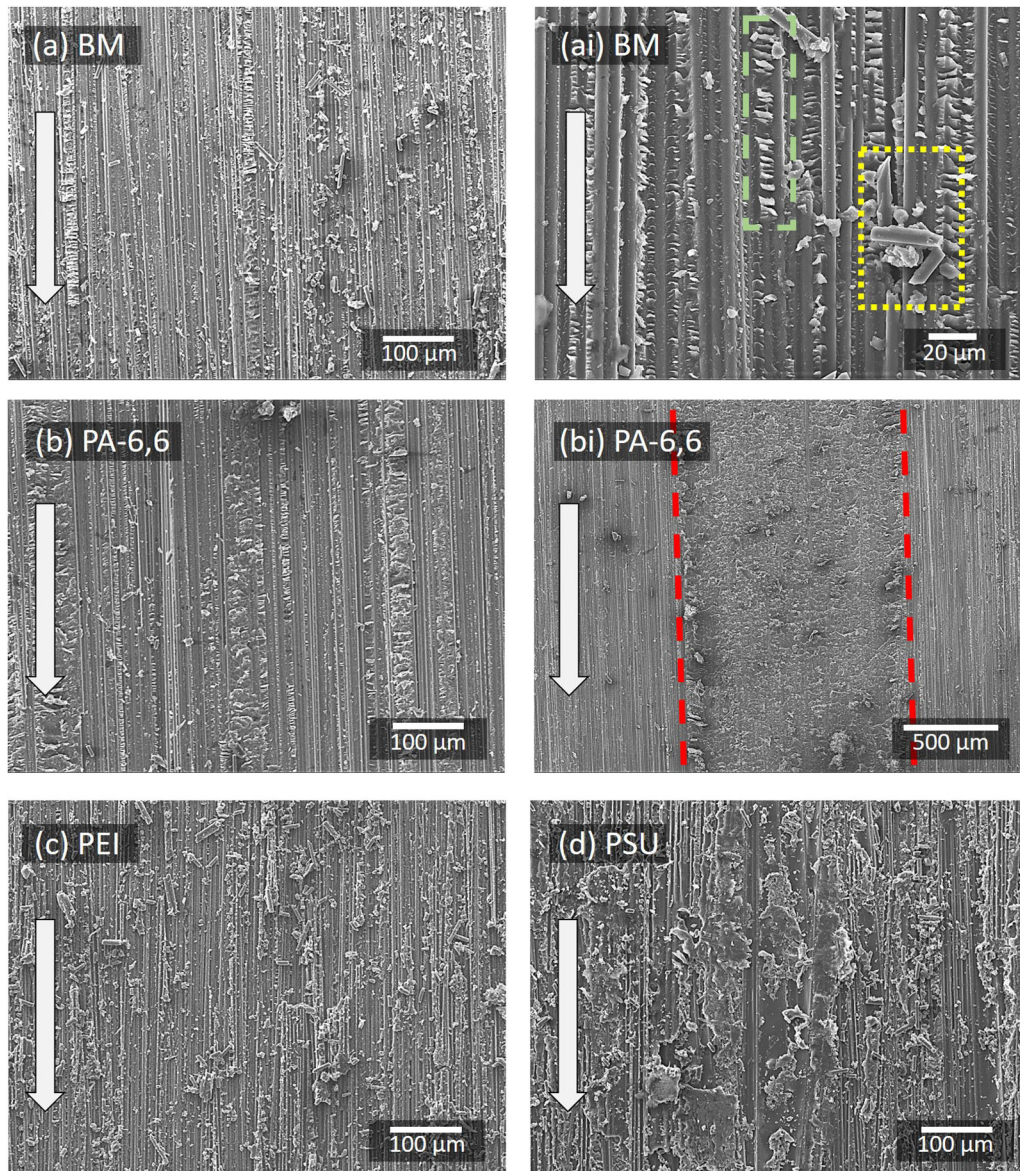


Figure 13. SEM images of the ENF fracture surfaces for (a) BM, (b) PA-6,6, (c) PEI, and (d) PSU. Green-dashed box highlights shear hackles; yellow dotted box highlights carbon fibre rupture and the red dashed lines highlight alternative failure mechanisms. The white arrow signifies the direction of crack propagation. (For interpretation of the references to colour in this figure legend, the reader is referred to the web version of this article).

within the reinforcement to improve mode I interlaminar toughness.

4. Conclusion

This article presents the effects on the interlaminar performance with the use of a commercial PA-6,6 along with electrospun PEI and PSU nanofibrous thermoplastic reinforcing interleaves. Two nanofibre veils (PEI and PSU) were fabricated in-house using an electrospinning rig to yield materials with areal weights an order of magnitude higher than the PA-6,6. Mode I tests were conducted in a DCB configuration and displayed improvements for all reinforced samples in $G_{IC,i}$, however, in propagation, the improvements reduced and in the case of the PA-6,6, the $G_{IC,i}$ was less than the benchmark. SEM

images of the cross-section and fracture surface suggest that the crack front is avoiding the reinforced interleaf for the PA-6,6, compared to the other reinforcements. Whilst this is at the detriment of mode I crack propagation, it favors mode II loading, with greater improvements observed compared to the PEI and PSU reinforcements. The $G_{IIc,i}$ results showed an improvement of 30% for the PA-6,6, a small improvement for the PEI and a reduction of 31% for the PSU. Further research is needed to see if the local interfacial chemistry or microstructure is changing in the vicinity of the veil, or if these veils can be used to direct and control crack propagation, leading to improved design of the failure modes of composites. As such, this article suggests a pathway for future design of composites with the intention of interlaminar toughness.

Acknowledgments

The authors would like to thank Robert Worboys (Bristol Composites Institute (ACCIS), University of Bristol) and the EPSRC, United Kingdom, Grant Numbers: EP/N006372/1, EP/I02946X/1 and EP/L02263X/1 for funding this research. The authors would also like to thank Revolution Fibres Ltd., New Zealand, for providing the Xantula[®] test samples and Solvay (Wilton, UK) for supplying the Udel[®] Bisphenol A polysulfone. SEM studies were carried out in the Chemical Imaging Facility, University of Bristol with equipment funded by EPSRC under Grant “Atoms to Applications” (EP/K035746/1).

Funding

This work was supported by the Engineering and Physical Sciences Research Council.

ORCID

T. R. Pozegic  <http://orcid.org/0000-0003-1707-4420>
 S. G. King  <http://orcid.org/0000-0001-6569-0338>
 M. Fotouhi  <http://orcid.org/0000-0002-5956-4703>
 V. Stolojan  <http://orcid.org/0000-0003-1137-4043>
 S. R. P. Silva  <http://orcid.org/0000-0002-0356-1319>
 I. Hamerton  <http://orcid.org/0000-0003-3113-0345>

References

- [1] Growth Opportunities in the Global Composites Industry. 2017. Available from: <http://www.lucintel.com/composites-industry-2017-2022.aspx>
- [2] Minak G, Palazzetti R, Trendafilova I, et al. Localization of a delamination and estimation of its length in a composite laminate beam by the VSHM and pattern recognition methods. *Mech Compos Mater*. 2010;46(4):387–394.
- [3] Shu D, Mai YW. Effect of stitching on interlaminar delamination extension in composite laminates. *Compos Sci Technol*. 1993;49(2):165–171.
- [4] Pozegic TR, Jayawardena KDGI, Chen JS, et al. Development of sizing-free multi-functional carbon fibre nanocomposites. *Compos Part A Appl Sci Manuf*. 2016;90:306–319.
- [5] Chan WS, Ochoa OO. Edge delamination resistance by a critical ply termination. *KEM*. 1991;37:285–303.
- [6] Xuefeng AN, Shuangying JI, Bangming T, et al. Toughness improvement of carbon laminates by periodic interleaving thin thermoplastic films. *J Mater Sci Lett*. 2002;21(22):1763–1765.
- [7] Howard WE, Gossard T, Jones RM. Reinforcement of composite laminate free edges with U-shaped caps. *AIAA Paper*. 1986;27(5):610–616.
- [8] Sela N, Ishai O. Interlaminar fracture toughness and toughening of laminated composite materials: a review. *Composites*. 1989;20(5):423–435.
- [9] Shivakumar K, Lingaiah S, Chen H, et al. Polymer nanofabric interleaved composite laminates. *AIAA J*. 2009;47(7):1723–1729.
- [10] Yudhanto A, Watanabe N, Iwahori Y, et al. Compression properties and damage mechanisms of stitched carbon/epoxy composites. *Compos Sci Technol*. 2013;86:52–60.
- [11] Dzenis YA, Reneker DH. Delamination resistant composites prepared by small diameter fiber reinforcement at ply interfaces. 2001. US6265333B1.
- [12] Beckermann GW, Pickering KL. Mode I and Mode II interlaminar fracture toughness of composite laminates interleaved with electrospun nanofibre veils. *Compos A Appl Sci Manuf*. 2015; 72:11–21.
- [13] Palazzetti R, Zucchelli A. Electrospun nanofibers as reinforcement for composite laminates materials – a review. *Compos Struct*. 2017;182:711–727.
- [14] Mirjalili M, Zohoori S. Review for application of electrospinning and electrospun nanofibers technology in textile industry. *J Nanostruct Chem*. 2016;6(3):207–213.
- [15] Navarro-Pardo F, Martinez-Hernandez AL, Velasco-Santos C. Carbon nanotube and graphene based polyamide electrospun nanocomposites: a review. *J Nanomater*. 2016;2016:1.
- [16] Liu Q, Zhu J, Zhang L, et al. Recent advances in energy materials by electrospinning. *Renew Sustain Energy Rev*. 2018;81:1825–1858.
- [17] Sundarrajan S, Tan KL, Lim SH, et al. Electrospun nanofibers for air filtration applications. *Procedia Eng*. 2014;75:159–163.
- [18] Khalf A, Madihally SV. Recent advances in multi-axial electrospinning for drug delivery. *Eur J Pharm Biopharm*. 2017;112:1–17.
- [19] O'Connor RA, McGuinness GB. Electrospun nanofibre bundles and yarns for tissue engineering applications: a review. *Proc Inst Mech Eng H*. 2016;230(11):987–998.
- [20] King SG, Stolojan V, Silva SRP. Large area uniform electrospun polymer nanofibres by balancing of the electrostatic field. *Reactive Funct Polymers*. 2017;129:89–94.
- [21] Christopherson GT, Song H, Mao H-Q. The influence of fiber diameter of electrospun substrates on neural stem cell differentiation and proliferation. *Biomaterials*. 2009;30(4):556–564.
- [22] Han W, Zheng G, Liang Y, et al. HDPE solution crystallization induced by electrospun PA66 nanofiber. *Colloid Polym Sci*. 2011;289(7):843–848.
- [23] King SG, McCafferty L, Stolojan V, et al. Highly aligned arrays of super resilient carbon nanotubes by steam purification. *Carbon*. 2015;84:130–137.
- [24] Daelemans L, van der Heijden S, De Baere I, et al. Nanofibre bridging as a toughening mechanism in carbon/epoxy composite laminates interleaved with electrospun polyamide nanofibrous veils. *Compos Sci Technol*. 2015;117:244–256.
- [25] Alessi S, Di Filippo M, Dispenza C, et al. Effects of Nylon 6,6 nanofibrous mats on thermal properties and delamination behavior of high performance CFRP laminates. *Polym Compos*. 2015;36(7): 1303–1313.
- [26] Saghafi H, Palazzetti R, Zucchelli A, et al. Influence of electrospun nanofibers on the interlaminar properties of unidirectional epoxy resin/glass fiber composite laminates. *J Reinforced Plastics Compos*. 2015;34(11):907–914.
- [27] van der Heijden S, Daelemans L, De Bruycker K, et al. Novel composite materials with tunable delamination resistance using functionalizable electrospun SBS fibers. *Compos Struct*. 2017;159: 12–20.

- [28] van der Heijden S, Daelemans L, De Schoenmaker B, et al. Interlaminar toughening of resin transfer moulded glass fibre epoxy laminates by polycaprolactone electrospun nanofibres. *Compos Sci Technol*. 2014;104:66–73.
- [29] Magniez K, De Lavigne C, Fox BL. The effects of molecular weight and polymorphism on the fracture and thermo-mechanical properties of a carbon-fibre composite modified by electrospun poly(vinylidene fluoride) membranes. *Polymer*. 2010; 51(12):2585–2596.
- [30] Daelemans L, van der Heijden S, De Baere I, et al. Damage-resistant composites using electrospun nanofibers: a multiscale analysis of the toughening mechanisms. *ACS Appl Mater Interf*. 2016;8(18): 11806–11818.
- [31] Liu L, Liang YM, Xu GY, et al. Mode I interlaminar fracture of composite laminates incorporating with ultrathin fibrous sheets. *J Reinforced Plastics Compos*. 2008;27(11):1147–1162.
- [32] Liu L, Huang Z-M, Xu G-Y, et al. Mode II interlaminar delamination of composite laminates incorporating with polymer ultrathin fibers. *Polym Compos*. 2008;29(3):285–292.
- [33] Beckermann GW. Nanofiber interleaving veils for improving the performance of composite laminates. *Reinforced Plastics*. 2017;61(5):289–293.
- [34] Johnson RO, Burlhis HS. Polyetherimide: a new high-performance thermoplastic resin. *J Polym Sci*. 1983;70(1):129–143.
- [35] R. F. Ltd. Available from: <http://www.revolutionfibres.com/wp-content/uploads/2014/03/Xantu-Layr-Product-Catalogue-v3.1.pdf>
- [36] Moon S, Choi J, Farris RJ. Preparation of aligned polyetherimide fiber by electrospinning. *J Appl Polym Sci*. 2008;109(2):691–694.
- [37] Saetia K, Schnorr JM, Mannarino MM, et al. Spray-layer-by-layer carbon nanotube/electrospun fiber electrodes for flexible chemiresistive sensor applications. *Adv Funct Mater*. 2014;24(4): 492–502.
- [38] Gopal R, Kaur S, Feng CY, et al. Electrospun nanofibrous polysulfone membranes as pre-filters: particulate removal. *J Membrane Sci*. 2007;289(1-2):210–219.
- [39] ASTM, D5528: Standard Test Method for Mode I Interlaminar Fracture Toughness of Unidirectional Fiber-Reinforced Polymer Matrix Composites. 2007.
- [40] Saghafi H, Zucchelli A, Palazzetti R, et al. The effect of interleaved composite nanofibrous mats on delamination behavior of polymeric composite materials. *Compos Struct*. 2014;109:41–47.
- [41] Ning H, Li Y, Hu N, et al. Improvement of the mode II interface fracture toughness of glass fiber reinforced plastics/aluminum laminates through vapor grown carbon fiber interleaves. *Sci Technol Adv Mater*. 2014;15(3):035004.
- [42] Czabaj MW, Ratcliffe JG. Comparison of intralaminar and interlaminar mode I fracture toughnesses of a unidirectional IM7/8552 carbon/epoxy composite. *Compos Sci Technol*. 2013;89:15–23.
- [43] Brugo T, Palazzetti R. The effect of thickness of nylon 6,6 nanofibrous mat on modes I–II fracture mechanics of UD and woven composite laminates. *Compos Struct*. 2016;154:172–178.
- [44] Kim K-Y, Ye L, Phoa K-M. Interlaminar fracture toughness of CF/PEI and GF/PEI composites at elevated temperatures. *Appl Compos Mater J*. 2004;11(3):173–190.
- [45] Li G, Li P, Zhang C, et al. Inhomogeneous toughening of carbon fiber/epoxy composite using electrospun polysulfone nanofibrous membranes by in situ phase separation. *Compos Sci Technol*. 2008; 68(3-4):987–994.